Gökhan Küçüktürk ✉
Hilal Akıllılar

https://doi.org/10.21278/TOF.464038121
ISSN 1333-1124
eISSN 1849-1391

INVESTIGATING THE EFFECT OF ELECTRON BEAM MELTING PARAMETERS ON THE Ti6Al4V ALLOY: A SIMULATION STUDY

Summary

Electron beam melting is one of few techniques that can melt powder directly; is a powder bed technique, classified as an additive manufacturing method. The electron beam melting method is based on melting the material to build a high-density solid part by applying a high-energy electron beam to a powder layer in a vacuum chamber. The parameters used during the electron beam melting process significantly affect the properties of the final part being printed. These parameters are beam power, spot size, scanning speed, and layer thickness. It is necessary to choose the best values for these parameters to increase the surface integrity of the part built. This study developed a computational fluid dynamics model with a moving Gaussian distribution electron beam source applied to one layer consisting of Ti6Al4V alloy powders. The model was solved with the ANSYS software to investigate the effects of the selected parameters. The results indicated that the temperature gradients, molten pool sizes, and melting-evaporation temperature ranges were determined by applying the parameter combinations used on the beam-powder interaction throughout the process. The simulation results have emphasised the outcomes determined by the power and scanning speed parameters that directly affect the molten pool dimensions. This way, the status of powder-beam interaction zones has been identified as either within or outside the melting-evaporation range.

Key words: *Electron beam melting; Ti6Al4V alloy; computational fluid dynamics; beam power; scanning speed*

1. Introduction

Recently, a process of producing parts layer by layer via 3D geometric design data has been developed from rapid prototyping to final geometry manufacturing among additive manufacturing methods [1, 2]. Additive manufacturing (AM), which was first used in the 1980s for rapid prototyping, has been developing for over 20 years and is among the most rapidly developed methods of recent times [3-4]. It has many advantages, such as ease of producing parts with complex geometries, lack of geometric design constraints, and low waste material formation [5-7]. Among additive manufacturing techniques, the electron beam melting (EBM) technique offers many unique features, such as higher energy efficiency, higher build rates due to increased penetration depths, higher scanning speeds, and moderate production costs. That is why many researchers have been studying the EBM technology, trying to further develop it for different applications [8, 9].

The Ti6Al4V alloy, the most widely used titanium-based alloy, has been preferred for AM technologies due to its benefits, such as low density, perfect biocompatibility, and high specific strength. Thanks to both the superior properties of the material and the flexibility of AM technologies, the Ti6Al4V alloy has many potential applications in a wide range of fields such as aerospace and automotive industries, and biomedicine [10-13].

Even though EBM has many advantages compared to conventional techniques, it also has some disadvantages, such as a lower degree of final product stability, lower surface quality, and product defects, because it is still being developed. Therefore, research into optimal process parameters and thermal phenomena are essential for the creation of an appropriate physical model of heat transfer and heat source [12]. Although there is a large number of experimental studies on EBM in the scientific literature, the number of studies on EBM parameters, such as modelling and simulation, remains limited. This is primarily due to the fact that the simulation of the EBM process is a highly complex process that is difficult to mathematically model; therefore, assumptions should be made to reduce its complexity [9].

Many previous studies focused on the EBM technique. Zah and Lutzman [5] investigated the effects of scanning speed and beam power parameters of EBM. In their research, a mathematical physical model was generated using the finite element analysis (FEA), and these results were used to simulate the effect of different parameters on the molten pool. Three different combinations of parameters were simulated, and the results, three molten pool geometries, were analysed, and then compared with each other. The simulations show that the molten pool dimensions significantly changed by increasing the scanning speed at a beam power of 150 W. In the conclusion of the comparison, it is reported that the molten pool size obtained with the parametric combination of a scanning speed of 50 mm/s and a beam power of 150 W is largest/smallest. Also, with this parametric combination, the molten pool geometries have the lowest length to width ratio. Shen and Chou [12] developed an FEA model, which was validated in the study of Wang et al. [14]. Their study used the generated model to simulate heat transfer in building parts produced with a tracing heat source with a Gaussian volumetric distribution in EBM. Then, they used the model to investigate the effects of the beam spot size and porosity on the molten pool geometry. The results show that the applied thermal energy and the porosity level of the pool substantially change the size of the molten pool. As the porosity increases, the temperature of the molten pool and, consequently, the penetration depth, increase. These results show that the porosity level affects the thermal conductivity of the powder layer. Moreover, it has been determined that the maximum temperature of the melt pool decreases by increasing the beam spot size and reducing the beam spot's intensity as another study parameter.

Numerical analysis studies demonstrated that fluid flow features could affect the simulation results obtained by the finite element methods. In these studies, it is implied that Computational Fluid Dynamics (CFD) could influence the modelling properties. Li et al. [15] studied the phase change in ceramic materials using the 3D numerical modelling in CFD for the laser surface melting method. Also, Rai et al. [16] used a numerical model that includes heat transfer and fluid flow to analyse the temperature distribution of the electron beam source in 304L powders. Both studies demonstrate that the heat transfer by convection from the molten pool was significant and influential in the computation of the molten pool size and shape. Rahman et al. [17] developed a CFD model for the Ti6Al4V powder; in the model, the powder layer is being scanned by a beam path for the EBM method. They investigated the properties of the molten pool, melting, and solidification in EBM.

Jamshidinia et al. [18] studied the temperature distribution of molten pool convection by modelling both CFD and FEM combinations to analyse the effect of different parameters. The study aims to investigate the effect of the EBM scanning speed on thermal stresses because non-uniform thermal distribution is the primary purpose of the study. In their study, Cheng et al. [19] researched different thermal characteristics of EBM using numerical and experimental methods.

They developed an extensive thermal model using finite element analysis software. They also used the model to analyse the effects of porosity on temperature profiles and molten pool sizes.

In study [9], a comparison with the literature was made by developing a 3D thermal model associated with the thermal properties of Ti6Al4V. The research was based on analysing the effects of the EBM process parameters on the molten pool geometry and temperature distribution alongside the powder layer. The Gaussian distribution beam source for EBM was designed with convenient parameter settings and applied to the powder layer within the baseplate scanning line. The heat source tracing a linear scanning pattern was applied to the scanned powder surface.

Extensive literature research demonstrates that there is a limited number of theoretical studies with simulations on the EBM method. In the study presented here, we developed mathematical equations using the CFD approaches and heat transfer principles. The simulations were conducted in the ANSYS Fluent software; the experimental and simulation results were compared with those presented in the literature and were validated in that way. The user-defined functions (UDFs) were developed, including temperature-dependent material properties, such as thermal conductivity and density, specific heat properties, and temperature-dependent equations. Besides, the model was first validated with the results presented in the study of Shen and Chou [12], and then, the results for different parameters obtained by the model were compared with each other and the results presented in the literature data.

2. Model Development

A beam tracing a linear path with a Gaussian profile is employed to model the EBM process. The simulation of distribution of electron beam heat input in the powder layer is modelled using the ANSYS software. The UDFs, embedded in the software, are designated for the beam source and material properties, including specific heat, thermal conduction, and density. The solidification and melting module of the software was applied; that helped to understand the fraction of the molten area over a unit area.

2.1 Heat Transfer Model

The generated UDF for the Ti6Al4V powder properties included the thermal conductivity, density, and specific heat; these properties are implemented in the model as a function of temperature, according to the experimental study [19]. Heat transfer, as a result of the interaction between the electron beam and the powder layer, is expressed by the following heat transfer equation:

$$\rho C_p \frac{\partial T}{\partial t} = \nabla \cdot (\mathrm{K} \nabla \mathrm{T}) + S_h \tag{1}$$

T, ρ, C_p, and K are the temperature, density, specific heat, and thermal conductivity of powder material, respectively; S is the term that is a description of the heat source, and in this case, electron beam source is assumed to have a Gaussian profile according to reference [20]:

$$S_h = A I_o \alpha \exp\left(-2\,\frac{(x-v_x t)^2+(y-v_y t)^2}{\omega^2} - \alpha z\right) \tag{2}$$

where A is the material absorptivity, α is the effective absorption coefficient, I_o is the electron beam intensity, ω is the electron beam characteristic radius, D_b is the diameter of the beam, and D_p is the powder mean diameter (D_{50}) [19]:

$$I_o = \frac{2P}{\pi\,\omega^2} \tag{3}$$

$$\omega = \frac{D_b}{2\times 2.146} \tag{4}$$

$$\alpha = \frac{1}{D_p} \tag{5}$$

Material properties of Ti6Al4V alloy as a function of temperature were considered in this study. The graphs of temperature-dependent density, thermal conductivity, and specific heat taken from the experimental study [12] are shown in Figure 1. In accordance with the literature, the emissivity of the Ti6Al4V alloy was regarded as 0.7. Also, the absorptivity is assumed as 0.9 according to Rouquette et al. [21]. The melting and solidification temperatures T_m and T_s are 1665 and 1605 °C, respectively [12, 22].

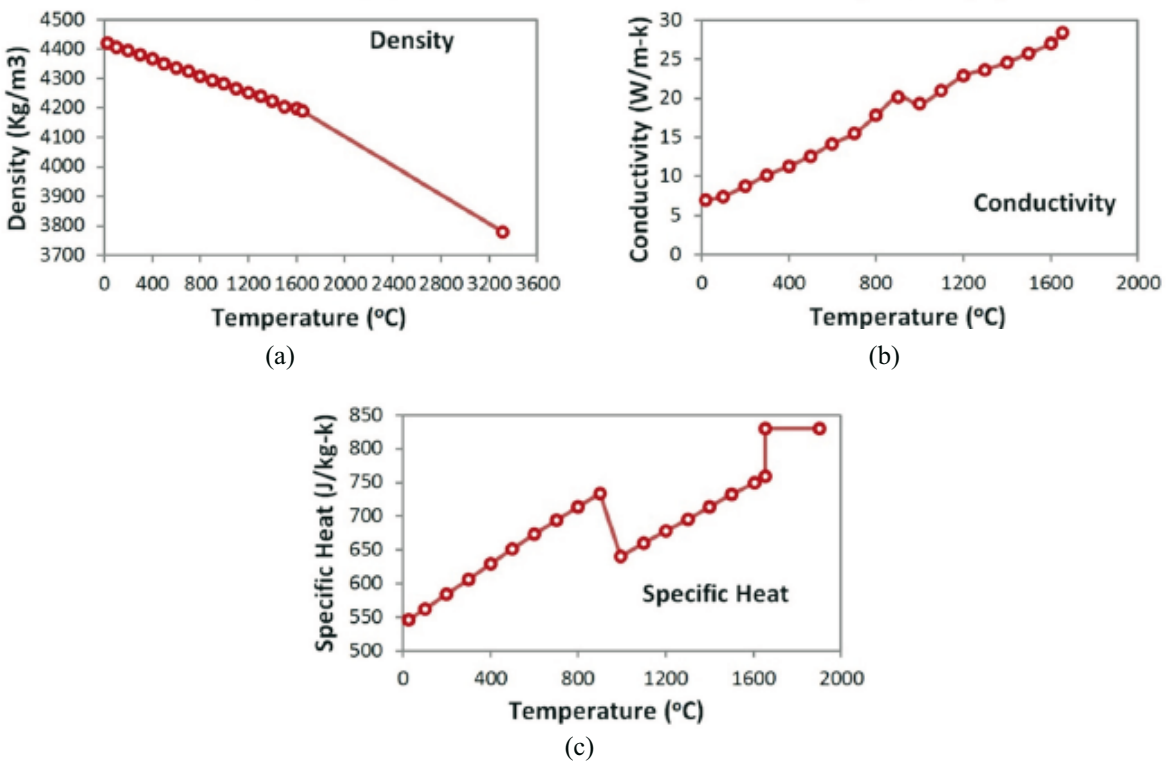

Fig. 1 Temperature-dependent properties of Ti-6Al-4V alloy, a) density, b) conductivity, c) specific heat [12]

2.2 Melting and Solidification Module

The enthalpy-porosity technique describes the melting and solidification that occur during EBM. The technique is based on enthalpy, which can be defined as the total heat in the system. Thus, enthalpy is equal to the sum of the internal energy of the system and the product of pressure and volume. In other words, it is the sum of sensible heat and the latent heat in the material. So we can write:

$$H = U + PV \quad \text{or,} \tag{6}$$

$$H = h + \Delta H, \tag{7}$$

where U, P, V, h, and ΔH are the internal energy, the pressure, the volume change, the sensible heat, and the latent heat, respectively. The sensible heat, h, and the latent heat, ΔH, can be expressed as:

$$h = h_{ref} + C_p \Delta T \tag{8}$$

$$\Delta H = \beta L, \tag{9}$$

where h_{ref}, L, $\boldsymbol{C_p}$, and β are the reference enthalpy, the latent heat, the specific heat, and the liquid fraction in the material, respectively. The liquid fraction β can be expressed as:

$$\beta = \frac{\mathrm{T-Tsolidus}}{\mathrm{Tliquidus-Tsolidus}} \tag{10}$$

Thus, using equation (10) , one can calculate the temperature T and use it to calculate the melting or solidification within the interaction zone.

2.3 Model Geometry and Numerical Solution

As mentioned, the electron beam source with several parameters, such as beam power, beam velocity, beam spot size, and scanning strategy, is modelled using a specific UDF code. The equations and the models are solved using ANSYS FLUENT. The material properties, described in Section 2.3, are also defined using UDF.

As the EBM process is conducted under the vacuum chamber condition, convection between the powder bed layer surface and the chamber environment should be ignored. Hence, only radiation was considered between the model and the surroundings. The uniform temperature distribution of $T_{preheat}$, 730 °C, has been assigned to the powder layer as the initial thermal condition. The model geometry used in the analysis is shown in Fig. 2.

The geometry comprises two rectangular parts of 4 mm in length and 4 mm in width. Also, for the thickness of the geometry, the first rectangular part with a thickness of 4 mm represents the base plate, and the second one represents the powder layer with a thickness of 50 µm.

As shown in Fig. 3, the mesh size at the current beam position of the layer is always very small in order to achieve more accurate results. The mesh size is smaller in the powder layer and gradually gets more prominent towards the bottom of the base plate. The number of elements for the thermal model is about 332800.

Figure 4 shows the computational domain for the model. The electron beam traces a linear way on top of the single powder layer with different power and velocity combinations shown in Table 1. The beam spot diameter is equal to 0.4 mm, the powder layer thickness is 50 µm, and it is constant. Table 2 shows other constant process parameters used.

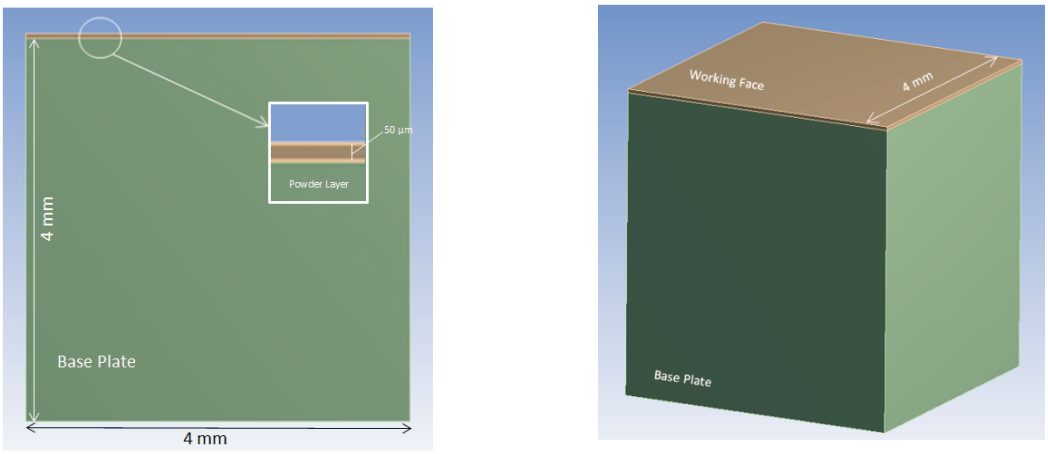

(a) (b)

Fig. 2 Model geometry of powder layer and base plate

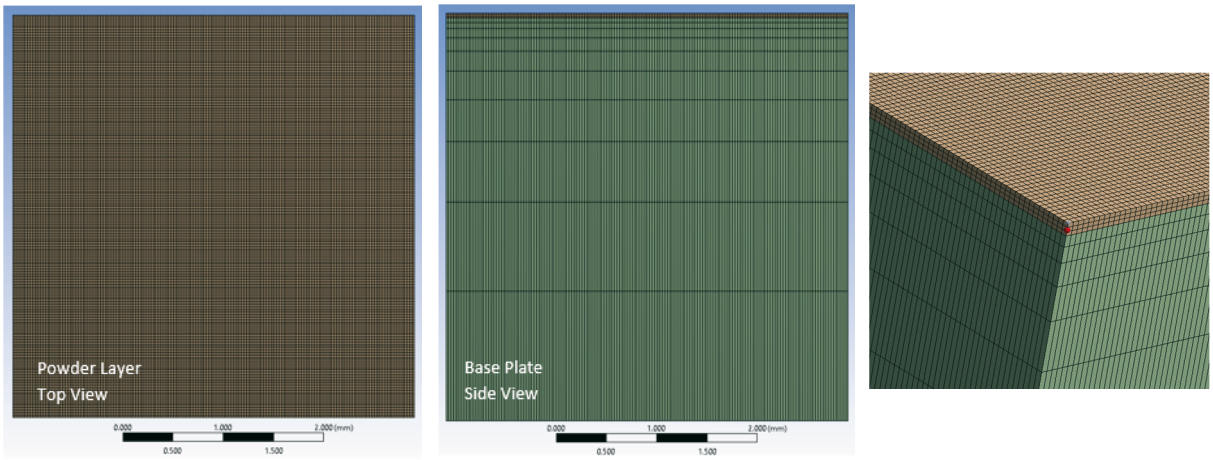

(a) (b) (c)

Fig. 3 Mesh for the geometry of, a) powder layer (top view), b) base plate (side view), c) powder layer and base plate combined (isometric view)

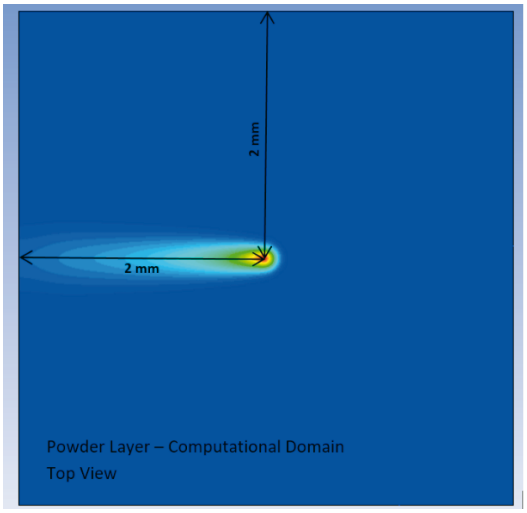

Fig. 4 Computational domain

Table 1 Parameter combinations

Power (W)	Velocity (m/s)														
	14	12	10	8	5.6	4	2.4	1.6	0.8	0.4	0.2	0.1	0.05	0.025	0.01
1750															
1500															
1250															
1000															
750															
500															

Table 2 Constant process parameters

PARAMETERS	VALUES
Solidus temperature T_S (°C)	1605 [12, 22]
Liquidus temperature T_L (°C)	1665 [12, 22]
Latent heat Lf (kJ/Kg K)	286 [23]
Absorption efficiency η	0.9
Accelerating voltage U (Kv)	60
Layer thickness t_{layer} (mm)	0.05
Electron beam diameter Φ (mm)	0.4
Beam penetration depth Dp (mm)	0.05
Preheating temperature $T_{preheat}$ (°C)	730 [19]

A schematic diagram of molten pool dimensions is shown in Fig. 5. The images indicate how to determine the dimensions of the molten pool. Fully melted parts were measured in the molten pool at the midpoint of the surface. The selected process parameters moderately affect the molten pool geometry.

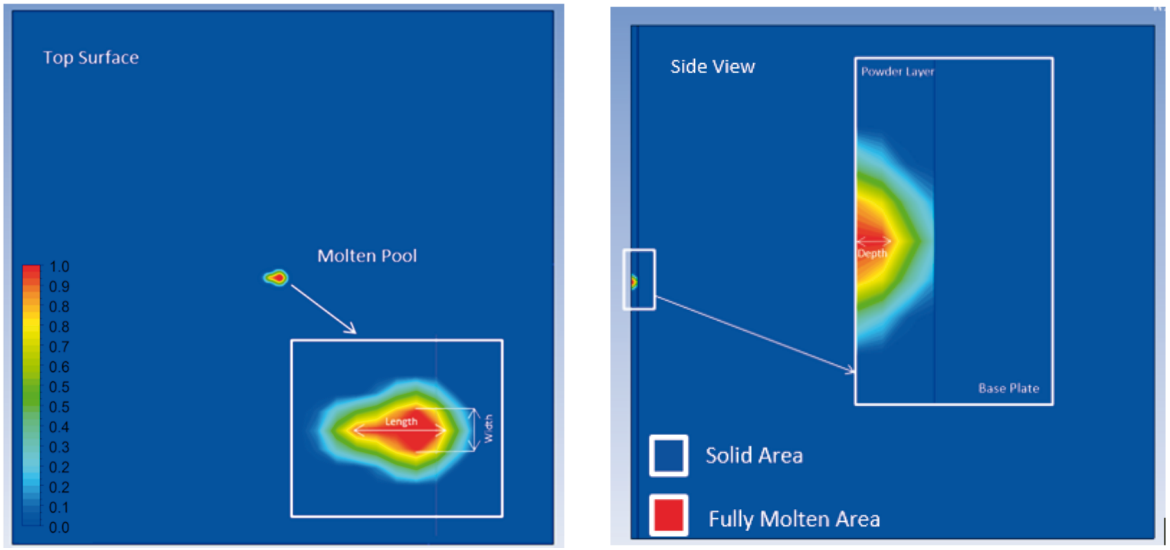

(a) (b)

Fig. 5 Dimensions of molten pool geometry: a) top surface, b) side view

2.4 Model Validation

Although it is better to carry experimental validation of the model, it was not done because of the lack of EBM experimental solutions; thus, the validation was performed using the results of Laser Engineered Net Shaping (LENS) presented in the study [14]. The LENS system has quite analogous configurations to EBM. Wang et al. investigated the molten pool geometry for the LENS process with an FEA model they developed. The authors used the experimental results obtained with the SS316 material, published in Hofmeister et al. [24], to validate their model.

The comparison of the correlation results is shown in Figure 6. Temperature gradients and the graphs of temperature profiles along the scanning path are compared. Figure 6 shows a close correlation between the experimental results obtained in Wang's study and those of our theoretical model.

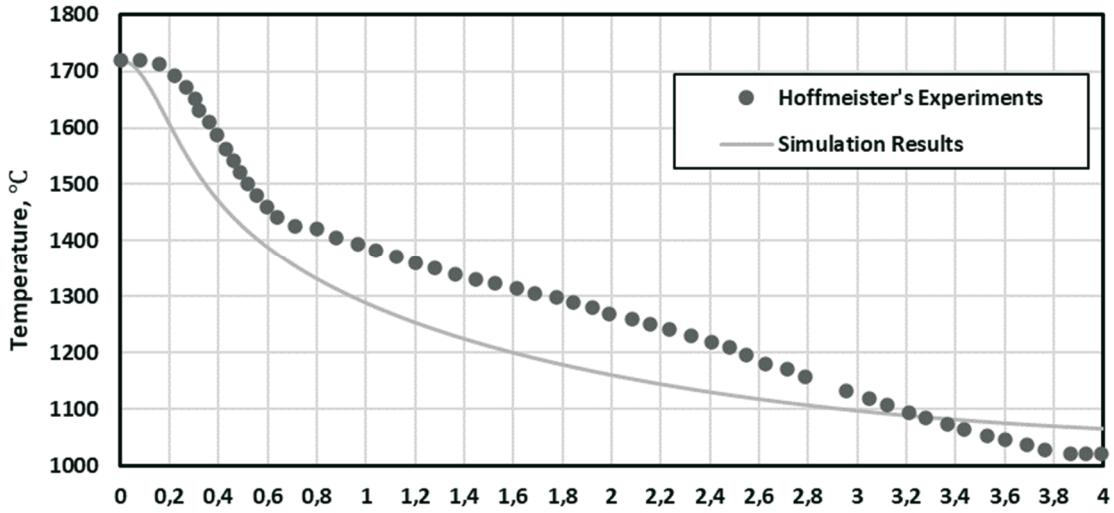

Fig. 6 Verified temperature profile along the beam centre scan pass

3. Results and Discussion

3.1 Beam Power Effect

Table 3 shows the side and top views of molten pool geometries and temperature distribution for different beam powers at 2.4 m/s. A higher maximum temperature is obtained with an increase in the beam power caused by increasing the energy density. The beam power affects the maximum temperature value, molten pool area, and heat penetration, which is characterised by the molten pool depth. The molten pool dimensions are compared in Table 6. One can note that it is quite easy for the high power electron beams to reach greater depths than a layer thickness of 50µm.

Table 3 Top and side views of molten pool and temperature distribution gradients at 2.4 m/s and different powers

2.4 m/s	Molten Pool	Temperature Distribution
1750W	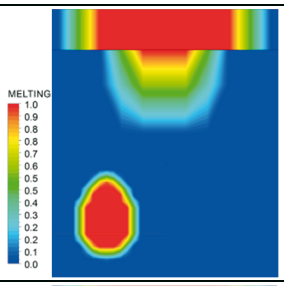	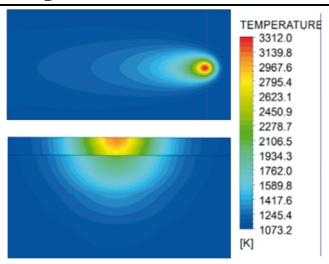
1500W	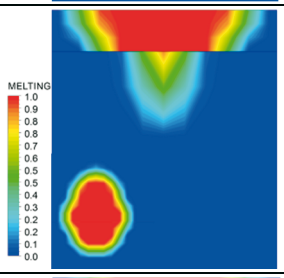	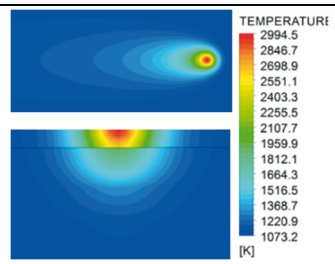
1250W	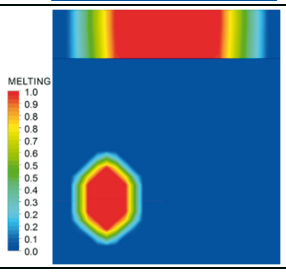	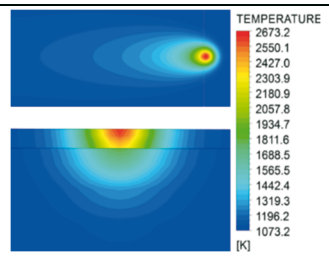

2.4 m/s	Molten Pool	Temperature Distribution
1000W	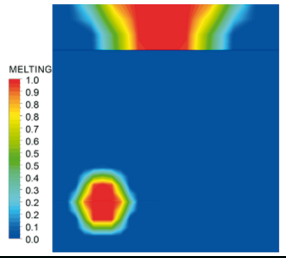	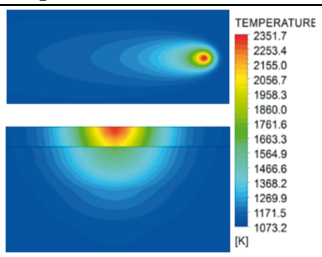
750W	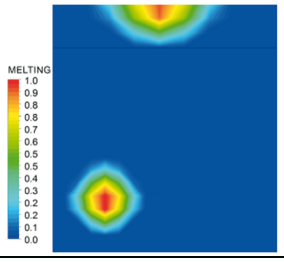	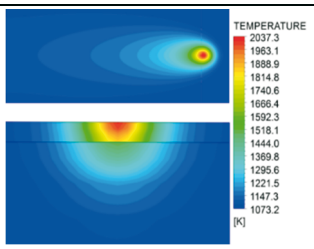

3.2 Scanning Speed Effect

Table 4 shows the side view and top view of melt pool geometries and temperature gradients for different scanning speeds at 1000W. Based on these results, one can conclude that a higher maximum temperature is reached more slowly because of excessive interaction time between the heat source and the layer. In addition, with a decrease in speed, temperature scales up, the molten pool dimensions increase, and heat penetration also increases. Besides, temperature gradients also get larger. The molten pool dimensions are compared in Table 6. For the increased scanning speeds, the molten pool depths are smaller than the layer thickness, which is 50 µm. We concluded that such a result is not convenient for the EBM experimental process.

Table 4 Top and side views of molten pool and temperature distribution gradients at 1000W and different speeds

1000 W	Molten Pool	Temperature Distribution
0.2 m/s		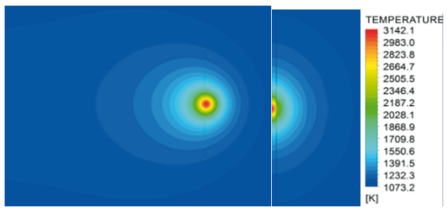
0.4 m/s	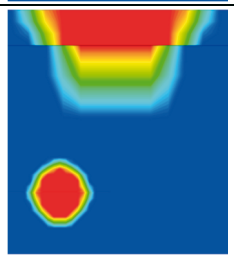	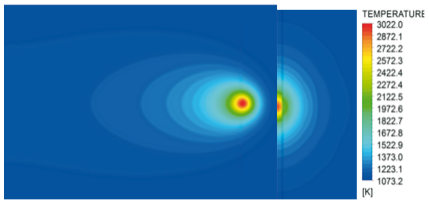
0.8 m/s	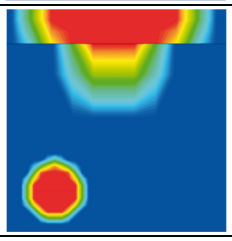	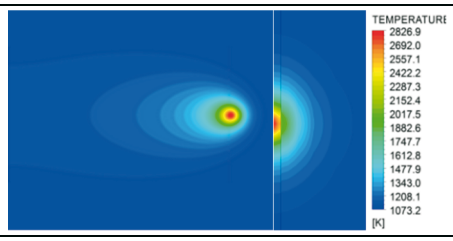

1000 W	Molten Pool	Temperature Distribution
1.6 m/s		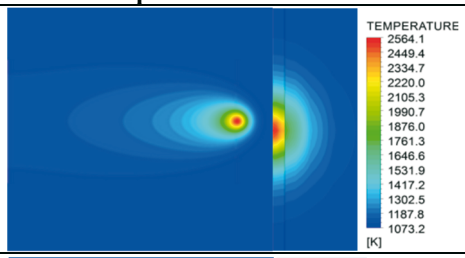
2.4 m/s	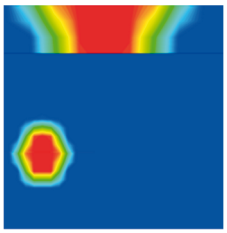	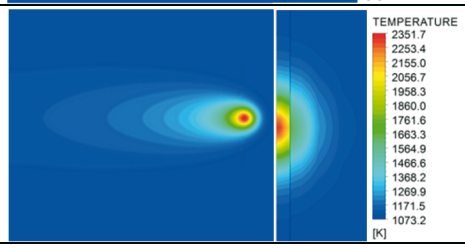
4 m/s	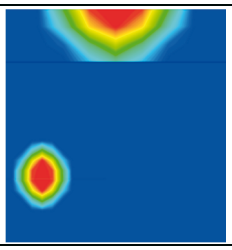	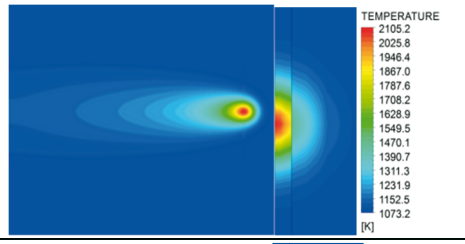
5.6 m/s	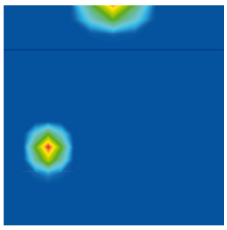	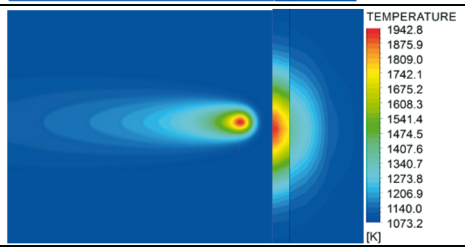

Table 5 shows the side and top views of the molten pool and temperature distribution gradients created by optimised maximum and minimum scanning speeds at powers of 1750 W and 1500 W. The parameters selected from the table significantly affected the temperature below the powder layer being processed. Whereas there is no complete melting within the molten pool area at higher speed values than 12 m/s for 1750 W, evaporation occurs within this area at speed values lower than 2.4 m/s for 1500 W. Similarly, the proper scanning velocities for complete melting within the molten pool area range between 10 and 1.6 m/s for a power of 1500 W.

Table 5 Side and top views of the molten pool and temperature distribution gradients of the maximum and minimum speeds at 1750 W and 1500 W.

1750W			1500W		
	Molten Pool	Temperature Distribution		Molten Pool	Temperature Distribution
12 m/s	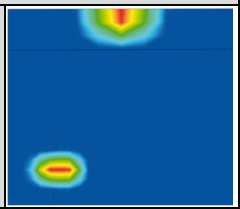	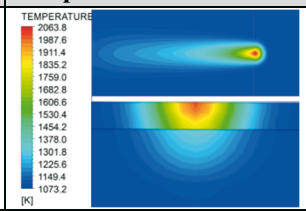	10 m/s	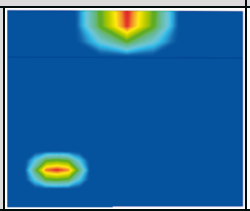	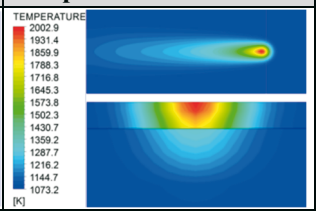
2.4 m/s	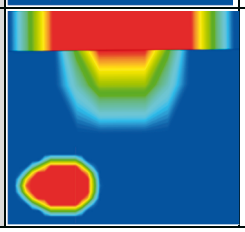	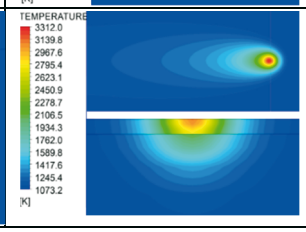	1.6 m/s	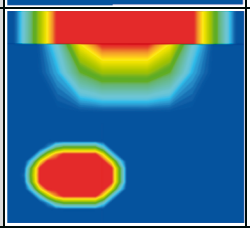	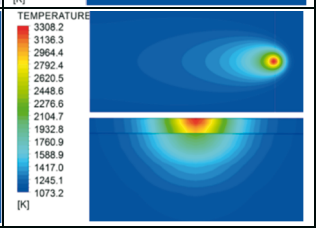

3.3 Melting and Evaporation Temperatures

Figures 7 and 8 show the temperature distribution from the centre of the beam on the scan path. The temperature measurement distance has been considered backwards 2 mm distance starting from the EBM beam centre of the heated path because of the heat being transferred into the powder layer and base plate by convection. The temperature levels between melting and evaporation lines for the different parameters are given in the graphs. For electron beam powers of 1250 W and 750 W, the graphs show the optimised speed values for melting and evaporation temperatures.

In Figure 8, one can see that speed values of less than 0.8 m/s cause evaporation in the molten pool area at 1250W; therefore, a speed of 0.4 m/s is not feasible for 1250 W. On the other hand, the powder layer cannot be melted at speeds above 5.6 m/s. So, a speed of 8 m/s is not relevant for melting the Ti6Al4V powder at a power of 1250 W.

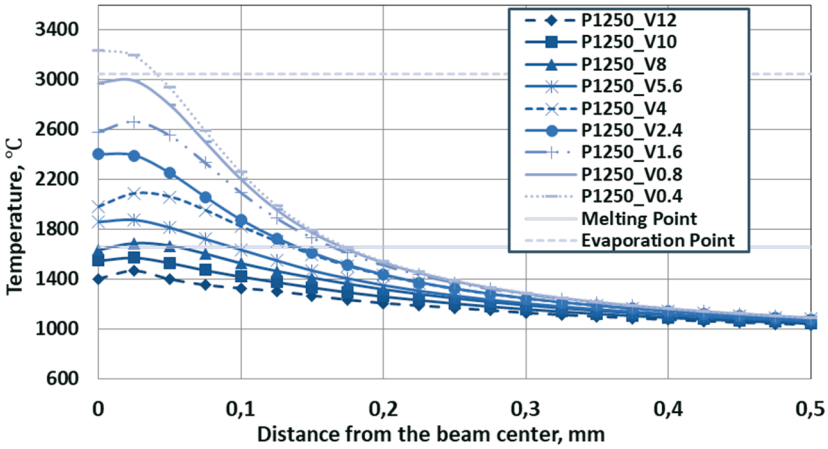

Fig. 7 Temperature distribution from the centre of the beam for 1250W

As shown in Figure 8, for the melting of powder, the minimum speed value of the electron beam for 750W must be lower than 4 m/s (starting from 2.4 m/s). The graph also shows there is no significant difference between speeds of 0.025 m/s, 0.05 m/s, and 0.1 m/s. Therefore, the speed must be low for this power, and these speed values are not feasible for experiments with EBM machines.

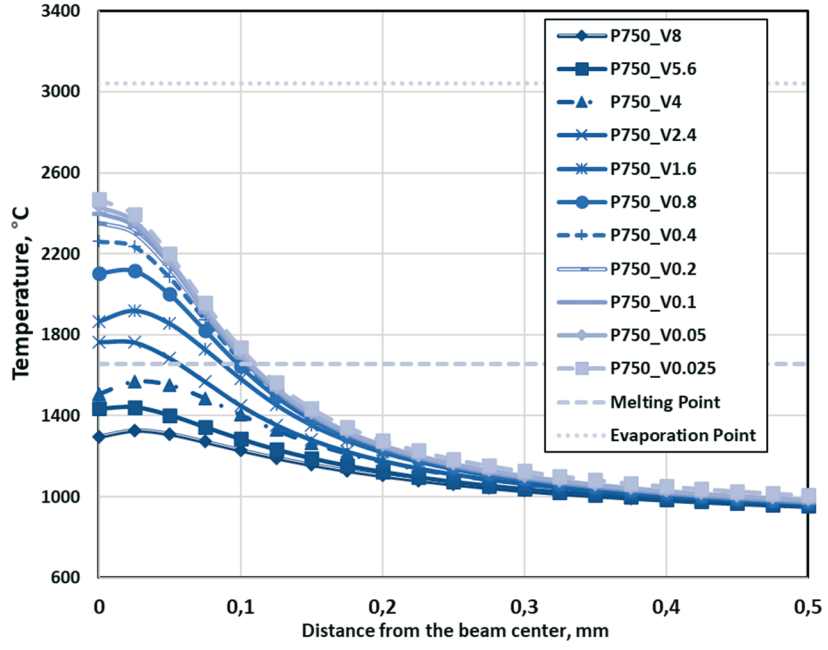

Fig. 8 Temperature distribution from the centre of the beam for 750W

Table 6 shows that differences in size of molten pool areas are small at lower speeds, such as 0.01 m/s, 0.025 m/s, and 0.05 m/s. It is clear to interpret the data shown in Table 6 that increasing the beam power value increases the dimensions of the molten pool area. Moreover, decreasing the speed of the beam results in increased molten pool dimensions.

Table 6 Molten pool dimensions for different parameters

1750W			1500 W			1250 W		
Velocity (m/s)	Width (μm)	Depth (μm)	Velocity (m/s)	Width (μm)	Depth (μm)	Velocity (m/s)	Width (μm)	Depth (μm)
14	2.56	7.91	12	2.38	1.35	8	2.36	1.54
12	3.0	16.5	10	3.66	9.18	5.6	50.90	19.8
10	45.4	19.4	8	52.2	19.0	4	54.10	50.0
8	53.2	50.0	5.6	53.7	49.1	2.4	102.0	50.0
5.6	103.0	50.0	4	104.0	50.0	1.6	153.0	50.0
4	110.0	50.0	2.4	153.0	54.3	0.8	203.0	53.0
2.4	155.0	53.1	1.6	173.0	55.0	0.4	210.0	54.0
1000W			750W			500W		
Velocity (m/s)	Width (μm)	Depth (μm)	Velocity (m/s)	Width (μm)	Depth (μm)	Velocity (m/s)	Width (μm)	Depth (μm)
5.6	3.15	1.45	2.4	8.2	17.9	0.8	4.58	3.47
4	42.0	18.0	1.6	53.1	49.2	0.4	33.4	20.30
2.4	68.1	50.0	0.8	103.0	50.0	0.2	56.0	34.00
1.6	103.0	50.0	0.4	112.0	50.0	0.1	57.4	50.00
0.8	153.0	53.0	0.2	155.0	53.0	0.05	58.0	50.00
0.4	163.0	53.5	0.1	158.0	53.6	0.025	64.0	50.00
0.2	203.0	54.0	0.05	158.0	57.0	0.01	104.0	50.00
-	-	-	0.025	159.0	58.0	-	-	-
-	-	-	0.01	207.0	60.0			

4. Conclusion

A model was developed and FEA simulations were carried out to understand the EBM source and powder interaction phenomena for Ti6Al4V. The main conclusions of this study are given below:

1. Scanning speed and beam power greatly affect the molten pool geometry and temperature distribution. As seen clearly from simulation results, when scanning speed is increased, the maximum temperature in the molten area is decreased.
2. For the lower beam power values, such as 750 W, the optimum speed for the melting temperature is relatively low, i.e., it is 2.4 m/s. Thus, it is hard to reach the evaporation temperature because, at a speed of 0.01 m/s, the temperature still cannot reach the evaporation temperature value. A speed lower than 0.01 m/s is not feasible for the experimental EBM procedure.
3. The energy density was calculated as the ratio of electron beam power (W) to electron beam scanning speed (m/s) for each condition. The highest density was obtained at a power of 750 W and a speed of 0.01 m/s. As a general conclusion, one can say that while power density directly affects the increase in the depth of the molten pool, it also affects the width of the pool indirectly. It was evaluated that this result is produced by the low heat transfer between the molten metal powders touching its surface areas.

REFERENCES

[1] Körner, C., Additive manufacturing of metallic components by selective electron beam melting – a review. International Materials Reviews, 2016. **61**(5): p. 361-377. https://doi.org/10.1080/09506608.2016.1176289

[2] Ramteke A.M., Ashtankar K.M., Sacrificial support fixture optimisation for the CNC rapid machining of medical parts with thin ends. Transactions of Famena, 2019. **43**(3), p. 65 – 82. https://doi.org/10.21278/TOF.43305

[3] Gu, D.D., et al., Laser additive manufacturing of metallic components: materials, processes and mechanisms. International Materials Reviews, 2012. **57**(3): p. 133-164. https://doi.org/10.1179/1743280411Y.0000000014

[4] Beaman, J. J., Bourell, D. L., Seepersad, C. C., and Kovar, D., Additive Manufacturing Review: Early Past to Current Practice, ASME. J. Manuf. Sci. Eng., November 2020; **142**(11): 110812. https://doi.org/10.1115/1.4048193

[5] Zäh, M.F. and Lutzmann, S., Modelling and simulation of electron beam melting. Production Engineering, 2010. **4**(1): p. 15-23. https://doi.org/10.1007/s11740-009-0197-6

[6] Vayre, B., F. Vignat, and F. Villeneuve, Metallic additive manufacturing: state-of-the-art review and prospects. Mechanics & Industry, 2012. **13**(2): p. 89-96. https://doi.org/10.1051/meca/2012003

[7] Zaharia S.M. et al., Mechanical properties and corrosion behaviour of 316l stainless steel honeycomb cellular cores manufactured by selective laser melting. Transactions of Famena, 2017. **41**(4), p. 11–24. https://doi.org/10.21278/TOF.41402

[8] Murr, L.E. et al., Microstructures and mechanical properties of electron beam-rapid manufactured Ti–6Al–4V biomedical prototypes compared to wrought Ti–6Al–4V. Materials Characterisation, 2009. **60**(2): p. 96-105. https://doi.org/10.1016/j.matchar.2008.07.006

[9] Gong, X., Anderson, T. and Chou, K., Int. Review on powder-based electron beam additive manufacturing technology. Manufacturing Review, 2014. https://doi.org/10.1051/mfreview/2014001

[10] Edwards, P., O'Conner, A. and Ramulu, M., Electron Beam Additive Manufacturing of Titanium Components: Properties and Performance. Journal of Manufacturing Science and Engineering, 2013. **135**(6). https://doi.org/10.1115/1.4025773

[11] Uhlmann, E., et al., Additive Manufacturing of Titanium Alloy for Aircraft Components. Procedia CIRP, 2015. **35**: p. 55-60. https://doi.org/10.1016/j.procir.2015.08.061

[12] Shen, N. and Chou, K., Thermal Modeling of Electron Beam Additive Manufacturing Process: Powder Sintering Effects. Proceedings of the ASME 2012 International Manufacturing Science and Engineering Conference collocated with the 40th North American Manufacturing Research Conference and in participation with the International Conference on Tribology Materials and Processing. ASME 2012 International Manufacturing Science and Engineering Conference. Notre Dame, Indiana, USA. June 4–8, 2012. p. 287-295. ASME. https://doi.org/10.1115/MSEC2012-7253

[13] Jakovljević S. et al., Investigation into the effects of laser texturing on the wettability of Ti-6Al-4V alloy. Transactions of Famena, 2021. **45**(4), p. 1-12. https://doi.org/10.21278/TOF.454031721

[14] Wang, L., et al., Optimisation of the LENS® process for steady molten pool size. Materials Science and Engineering: A, 2008. **474**(1): p. 148-156. https://doi.org/10.1016/j.msea.2007.04.119

[15] Li, J.F., Li, L. and Stott, F.H., A three-dimensional numerical model for a convection–diffusion phase change process during laser melting of ceramic materials. International Journal of Heat and Mass Transfer, 2004. **47**(25): p. 5523-5539. https://doi.org/10.1016/j.ijheatmasstransfer.2004.07.024

[16] Rai, R., et al., Heat transfer and fluid flow during electron beam welding of 21Cr–6Ni–9Mn steel and Ti–6Al–4V alloy. Journal of Physics D: Applied Physics, 2008. **42**(2): p. 025503. https://doi.org/10.1088/0022-3727/42/2/025503

[17] Rahman, M.S., Schilling, P.J., Herrington, P.D., and Chakravarty, U.K., A Comparative Study Between Selective Laser Melting and Electron Beam Additive Manufacturing Based on Thermal Modeling. Proceedings of the ASME 2018 International Mechanical Engineering Congress and Exposition. Volume 1: Advances in Aerospace Technology. Pittsburgh, Pennsylvania, USA. November 9–15, 2018. V001T03A015. ASME. https://doi.org/10.1115/IMECE2018-86428

[18] Jamshidinia, M., Kong, F. and Kovacevic, R., The Coupled CFD-FEM Model of Electron Beam Melting® (EBM). 2013.

[19] Price, S., et al., On Process Temperature in Powder-Bed Electron Beam Additive Manufacturing: Process Parameter Effects. Journal of Manufacturing Science and Engineering, 2014. **136**(6). https://doi.org/10.1115/1.4028485

[20] Cline, H.E. and Anth,ony, T.R. Heat treating and melting material with a scanning laser or electron beam. Journal of Applied Physics, 1977. **48**(9): p. 3895-3900. https://doi.org/10.1063/1.324261

[21] Rouquette, S., Guo, J. and Le Masson, P., Estimation of the parameters of a Gaussian heat source by the Levenberg–Marquardt method: Application to the electron beam welding. International Journal of Thermal Sciences, 2007. **46**(2): p. 128-138. https://doi.org/10.1016/j.ijthermalsci.2006.04.015

[22] Boyer, R., Welsch, G., and Collings, E. W., Materials Properties Handbook: Titanium Alloys. 1998: ASM International.

[23] Jamshidinia, M., Kong, F. and Kovacevic, R., Numerical Modeling of Heat Distribution in the Electron Beam Melting® of Ti-6Al-4V. Journal of Manufacturing Science and Engineering, 2013. **135**(6). https://doi.org/10.1115/1.4025746

[24] Ensz, M., Griffith, M., Hofmeister, W., Philliber, J.A., Smugeresky, J., and Wert, M. (Jun 1999). Investigation of Solidification in the Laser Engineered Net shaping (LENS) Process (SAND--99-1550J). United States

Submitted: 27.12.2021

Accepted: 25.7.2022

Gökhan Küçüktürk*
Gazi University, Faculty of Engineering, Department of Mechanical Engineering, Ankara, Turkey

Hilal Akıllılar
Gazi University, Graduate School of Natural and Applied Sciences, Department of Mechanical Engineering, Ankara, Turkey

*Corresponding author:
gkucukturk@gazi.edu.tr